Cavity-enhanced broadband photonic Rabi oscillation

Rikizo Ikuta,[1,2,*] Toshiki Kobayashi,[1,2] Tomohiro Yamazaki ⬤,[1] Nobuyuki Imoto,[2] and Takashi Yamamoto[1,2]

[1]*Graduate School of Engineering Science, Osaka University, Toyonaka, Osaka 560-8531, Japan*
[2]*Center for Quantum Information and Quantum Biology, Osaka University, Osaka 560-8531, Japan*

A coherent coupling among different energy photons provided by nonlinear optical interaction is regarded as a photonic version of the Rabi oscillation. Cavity enhancement of the nonlinearity reduces an energy requirement significantly and pushes the scalability of the frequency-encoded photonic circuit based on the photonic Rabi oscillation. However, the confinement of the photons in the cavity severely limits the number of interactable frequency modes. Here we demonstrate a wide-bandwidth and efficient photonic Rabi oscillation achieving full-cycle oscillation based on a cavity-enhanced nonlinear optical interaction with a monolithic integration. We also show its versatile manipulation beyond the frequency degree of freedom such as an all-optical control for polarizing photons with geometric phase. Our results will open up full control accessible to synthetic dimensional photonic systems over wide frequency modes as well as a large-scale photonic quantum information processing.

I. INTRODUCTION

Rabi oscillation, which is a cyclic rotation between coherently coupled two atomic levels driven by an optical field, is one of the most fundamental building blocks in atomic physics, and has been used for numerous technologies such as atomic clocks [1], sensors [2], quantum communication [3], and computing [4,5]. In a photonic system, the coherent two-level system is implemented by two distinct photonic frequencies coupled by nonlinear optical interaction with a pump light. Recently, such a photonic Rabi oscillation has been applied to a single photon known as quantum frequency conversion (QFC) [6] in quantum information processing, which can create a coherent superposition of the frequency modes in the single photon. Apart from atomic systems using naturally determined energy levels, the photonic systems use virtual levels determined by the pump frequency corresponding to the difference of the two frequencies [Fig. 1(a)]. This feature allows for interaction of densely embedded optical frequency modes over a wide range, and offers flexible manipulation of photonic frequencies that form the inherently equipped high-dimensional Hilbert space.

So far, several experimental demonstrations of quantum operations on the frequency-encoded qubits based on optical nonlinearities have been performed [7–9] aiming at frequency-domain photonic quantum information processing such as universal quantum computation based on multistage nonlinear optical interaction with the photonic Rabi oscillation [10–12]. Typically, the full Rabi cycle in $\chi^{(2)}$-based QFC corresponding to the so-called 2π pulse needs over a watt-class continuous wave (cw) pump power even when waveguided crystals are used [13–19]. Much more pump power is required for QFCs with bulk crystals or $\chi^{(3)}$ media due to shorter interaction time or smaller nonlinearity.

This prevents the scalable integration of the photonic Rabi oscillation for simulating more complex quantum systems. A promising approach for saving the cw pump power is an enhancement of optical nonlinearity by using an optical cavity. However, cavity systems in which all relevant lights are confined such as ring resonator systems [20,21] severely limit accessible frequencies and bandwidths of the photons, which sacrifices the feature of the photonic Rabi oscillation.

In this study, without losing the acceptable frequencies and bandwidth, we demonstrate cavity enhancement of the photonic Rabi oscillation by using laser lights toward the wideband and efficient QFC. We utilize a periodically poled lithium niobate (PPLN) waveguide as a $\chi^{(2)}$ medium with a cavity *only for* the pump light [Fig. 1(b)], which we call the PPLN waveguide resonator (PPLN/WR) hereafter. Compared with the QFC experiment without the cavity [13], the internal enhancement factor was estimated to be near 10 with achieving a maximum transition probability over 90 %, while the observed bandwidth was 176 GHz which is comparable with the reported value. Such an efficient photonic Rabi oscillation realized the full cycle of the coherent rotation between the two frequency modes. This also enables an all-optical control of polarizing photons beyond the manipulation of frequency degree of freedom (DOF). Thanks to the broad bandwidth property, we can simultaneously perform the operation over several dozen frequencies and polarizing modes forming hyperentangled states on dense quantum frequency combs [22,23].

II. THEORY

We explain the quantum theory of $\chi^{(2)}$-based photonic Rabi oscillation between angular frequencies ω_g and ω_e driven by a pump light at an angular frequency $\omega_p (= \omega_e - \omega_g)$ for the nonlinear optical interaction [13]. The subscripts of the two energy levels "e" and "g" mean "excited" and "ground" frequencies. The energy diagram relevant to the process is

─────────
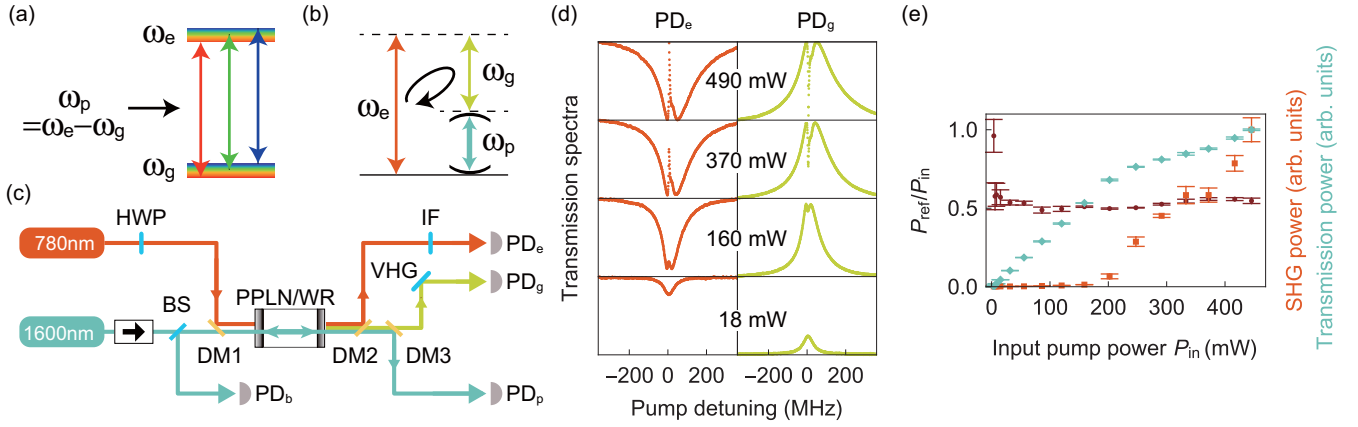*Corresponding author: ikuta@mp.es.osaka-u.ac.jp

FIG. 1. (a) Two-level photonic systems coherently coupled by photonic Rabi oscillation. Due to the virtual level structure, the ground and excited levels are regarded as continuously distributed. (b) Energy diagram of $\chi^{(2)}$ interaction equivalent to the coherent two-level systems. The pump light at angular frequency ω_p is confined in the cavity. (c) Experimental setup. The wavelengths 1600 nm and 780 nm correspond to the pump frequency ω_p and the excited state frequency ω_e, respectively; 1522 nm corresponds to the ground-state frequency $\omega_g (= \omega_e - \omega_p)$. HWP, half wave plate; BS, beamsplitter. Other acronyms are defined in the main text. (d) Input pump power dependencies of the transmission spectra of 780 nm light and 1522 nm light. The power in the figure is the input pump power measured in front of the PPLN/WR. (e) Input pump power dependencies of the ratio of the reflected pump power to the input pump power (P_{ref}/P_{in}) (brown circle, left-hand axis), and SHG/transmission power of the pump light (orange square/light blue diamond, right-hand axis). The error bars indicate one standard deviation. For estimating the mode matching, we used the data with the standard deviations smaller than 5 % (the four leftmost data are omitted).

shown in Fig. 1(b). When the pump light is sufficiently strong, and the perfect phase matching condition is satisfied, the effective Hamiltonian is described by $H = i\hbar(g^* a_e^\dagger a_g - g a_e a_g^\dagger)$, where $a_{e(g)}$ is an annihilation operator of the higher (lower) frequency mode. The effective coupling constant $g = |g|e^{i\phi}$ is proportional to the complex amplitude of the pump light with phase ϕ. From this Hamiltonian, annihilation operators $a_{e,out}$ and $a_{g,out}$ for the higher and lower frequency modes from the nonlinear optical medium are described by

$$\begin{bmatrix} a_{e,out} \\ a_{g,out} \end{bmatrix} = \begin{bmatrix} \cos\frac{\theta}{2} & -e^{i\phi}\sin\frac{\theta}{2} \\ e^{-i\phi}\sin\frac{\theta}{2} & \cos\frac{\theta}{2} \end{bmatrix} \begin{bmatrix} a_e \\ a_g \end{bmatrix}, \quad (1)$$

where $\theta/2 = |g|\tau$, and τ is the interaction time of the light through the nonlinear optical medium. This process is equivalent to the atomic Rabi oscillation driven by the external optical field resonant with the two energy levels. The branching ratio of the transition matrix can be adjusted by the pump power. We notice that at $\theta = 2\pi$, the light at the initial frequency mode is obtained with a unit probability, while the π phase shift understood by the geometric phase is added to its complex amplitude. When the nonlinear optical medium is placed inside a cavity confining only the pump light, the coupling strength $|g|$ is enhanced, resulting in a higher Rabi frequency while preserving the intrinsic bandwidth of the nonlinear interaction. On the other hand, the cavity confinement may induce a constant shift of phase ϕ in Eq. (1), which gives no adverse effect in the experiment.

III. EXPERIMENTAL SETUP

The experimental setup for the photonic Rabi oscillation between 780 and 1522 nm light driven by the cavity-enhanced pump light at 1600 nm is shown in Fig. 1(c). The cw pump light and the 780 nm light with a power of 1 mW are combined at a dichroic mirror (DM1), and then focused on the

PPLN/WR. The coupling efficiency of 780 nm light to the PPLN/WR is 0.91.

The details of the PPLN/WR used in our experiment are described as follows. The PPLN waveguide is a similar design to the one used in Ref. [13]. It is a ridged-type waveguide with 8-μm width. The periodically poling period is about 18 μm for satisfying the type-0 quasi-phase-matching condition, and the polarization of the light relevant to the Rabi oscillation is vertical (V). The length of the waveguide is 20 mm. For forming the singly resonant PPLN waveguide resonator with the Fabry-Pérot structure, the end faces of the waveguide are flat polished, and directly coated by dielectric multilayers. The reflectance for 1600 nm at both end faces of the waveguide is 97.6 %. The observed full width at the half maximum (FWHM) and the quality factor of the cavity are about $\Delta = 60$ MHz and 3.2×10^6 [23], respectively. For 780 nm and 1522 nm, antireflective coatings at the front (back) ends of the waveguide are achieved with the reflectances of $\sim$0.6 (0.2)% and $\sim$14 (5)%, respectively.

After the PPLN/WR, the 780 nm light is reflected by DM2, and passes through an interference filter (IF) with a bandwidth of 3 nm followed by a photodetector (PD$_e$). The 1522 nm light and the pump light pass through DM2, and they are separated by DM3. The 1522 nm light passing through DM3 is diffracted at a volume holographic grating (VHG) with a bandwidth of 1 nm and is detected by PD$_g$. The pump light reflected at DM3 is detected by PD$_p$. The pump light coming back from the PPLN/WR is monitored by PD$_b$.

IV. EXPERIMENTAL RESULTS

A. Cavity-enhanced photonic Rabi oscillation with broadband property

The branching ratio between the two frequency modes characterized by rotation angle θ of Rabi oscillation in Eq. (1)

was measured by the PDs for various pump powers while scanning the pump frequency. Examples of the observed power spectra for 780 nm and 1522 nm light are shown in Fig. 1(d). We see that when the pump light was resonant to the PPLN/WR, the transition process was observed as a dip and a peak of the power spectra. For the pump power satisfying $0 \leqslant \theta \leqslant \pi$, a higher pump power leads to a deeper dip and a higher peak of the spectra (the bottom figure). For the pump power such that $\theta > \pi$ is satisfied (the other three figures), the dip at 780 nm and the peak at 1522 nm were, respectively, turned into upward and downward. This behavior shows the frequency recovery from 1522 nm to 780 nm after the transition from 780 nm to 1522 nm.

The input pump power $P_{\rm in}$ was measured just before the PPLN/WR. In order to estimate an effective pump power P coupled to the resonator, we measured the ratio of the reflected pump power $P_{\rm ref}$ to $P_{\rm in}$ from the reflection spectra at PD_b for the estimation of the mode matching coefficient M, and second harmonic generation (SHG) at 800 nm of the pump light at PD_e for the estimation of an unexpected nonlinear optical effect. We show the experimental results in Fig. 1(e). $P_{\rm ref}/P_{\rm in}$ is estimated to be 0.52 on average, which reflects amounts of the mode mismatched portion $1 - M$ and the back reflection of the pump light coupled to the resonator. The latter is determined by $(1 - \Delta_0/\Delta)^2 \sim 0.30$ [24], where $\Delta_0 = 27\,{\rm MHz}$ is the FWHM determined by the symmetric reflectance 97.6 % at the ends of the resonator with no internal photon loss. By solving $0.30M + (1 - M) = 0.52$, M is estimated to be 0.69. From this value and the reflected pump spectra, we determined the effective coupled pump power P. We note that the SHG power gradually increases as shown in Fig. 1(e). Corresponding to this, the transmitted pump power measured by PD_p begins to deviate from the proportional relationship with the input pump power. This indicates that the coupled pump power is consumed by SHG, which may shift the amount of the back reflection portion of the pump light. But the roughly constant values of $P_{\rm ref}/P_{\rm in}$ show such influence is small enough for the above estimation.

Together with the estimated values of P and the observed spectra of 780 nm and 1522 nm light, we plot the staying probability (transmittance) $T(P)$ and the transition probability (reflectance) $R(P)(:= 1 - T(P))$ in Fig. 2(a) based on the normalization method in Refs. [7,25]. The maximum transition probability corresponding to the π pulse was achieved at $\sim$80 mW pump power. By using the observed values for <200 mW pump power in which SHG is negligibly small from Fig. 1(e), the best fit to $T(P)$ with a function $1 - A\sin^2(\sqrt{BPL})$ gives $A = 0.92$ and $B = 0.078\,{\rm W}^{-1}{\rm mm}^{-2}$, where $L = 20$ mm is the waveguide length. This result is used for the dashed curves in Fig. 2(a). By using the parameters, we plot $T(P)$ and $R(P)$ vs $\theta(P)$ in Fig. 2(b), which shows the clear Rabi oscillation achieving full cycle.

The pump light confinement in the Fabry-Pérot cavity allows for the Rabi oscillation regardless of the input direction of the pump light. To see this, we swapped the positions of the 780-nm light source and the detector PD_e. The experimental result is shown in Figs. 2(c) and 2(d). As is expected, the oscillation of the frequency transition was surely observed. The best fit to $T(P)$ with $1 - A'\sin^2(\sqrt{B'PL})$ gives $A' = 0.95$ and $B' = 0.075\,{\rm W}^{-1}{\rm mm}^{-2}$, which is used for the dashed curves in
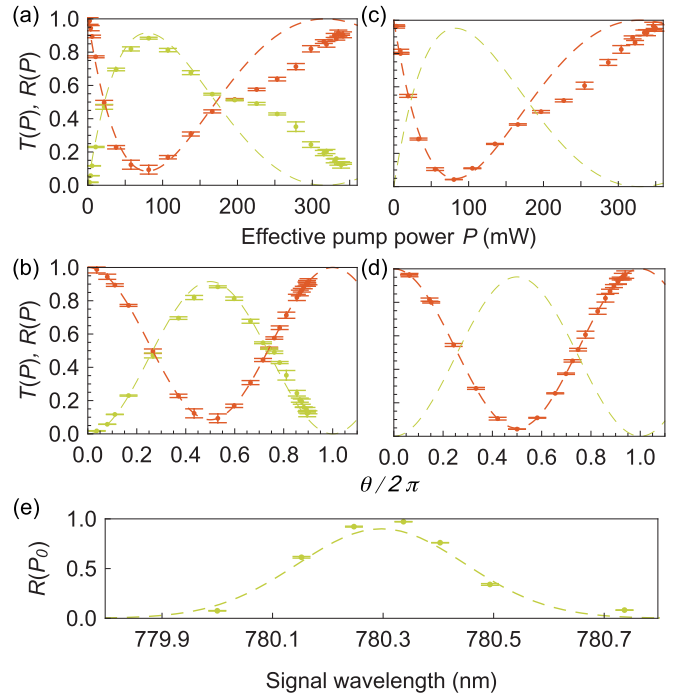

FIG. 2. (a)–(d) $T(P)$ (red) and $R(P)$ (green) vs P and $\theta/(2\pi)$. (a) and (b) For the signal light coming from the direction same as the pump light. The dashed curves for $T(P)$ and $R(P)$ are functions $1 - A\sin^2(\sqrt{BPL})$ and $A\sin^2(\sqrt{BPL})$, respectively, where $A = 0.92$, $B = 0.078\,{\rm W}^{-1}{\rm mm}^{-2}$. θ is estimated by $\theta(P) = 2\sqrt{BPL}$. (c) and (d) For the signal light coming from the direction opposite the pump light. The dashed curves for $T(P)$ and $R(P)$ are functions $1 - A'\sin^2(\sqrt{B'PL})$ and $A'\sin^2(\sqrt{B'PL})$, respectively, where $A' = 0.95$, $B' = 0.075\,{\rm W}^{-1}{\rm mm}^{-2}$. θ is estimated by $\theta(P) = 2\sqrt{B'PL}$. (e) The observed transition probability vs the signal wavelength for $P_0 \sim 80$mW.

the figures. These estimated values are similar to A and B, and the bidirectional photonic Rabi oscillation was successfully achieved.

To see the amount of the cavity enhancement, we compare the value of the normalized coupling constant $B = 0.078\,{\rm W}^{-1}{\rm mm}^{-2}$ with the values in previously reported papers. In Ref. [13], the QFC system including the PPLN waveguide and wavelengths of the relevant light is almost the same as this experimental setup except for the cavity coating. The value of the coupling constant is calculated to be $0.009\,{\rm W}^{-1}{\rm mm}^{-2}$ from the reported experimental data. From these results, an enhancement factor of the coupling constant is estimated to be 8.6. This value agrees well with a theoretical value [26,27] $F_{\rm obs}^2/(\pi F_0) \sim 8.4$ where $F_{\rm obs}$ and F_0 are finesses $F_{\rm obs} = \nu_{\rm FSR}/\Delta = 59$ and $F_0 = \nu_{\rm FSR}/\Delta_0 = 130$ with the free spectral range $\nu_{\rm FSR} = 3.5\,{\rm GHz}$ [28]. Compared to other QFC experiments using PPLN waveguides without cavities in various situations [14–19] in which the coupling constant is from 0.003 to $0.012\,{\rm W}^{-1}{\rm mm}^{-2}$, our result shows a significant enhancement by the cavity.

Next, we measured the bandwidth of the photonic Rabi oscillation by setting the effective pump power to $P \sim 80\,{\rm mW}(=: P_0)$. The observed transition probabilities for various signal wavelengths around 780 nm were shown in
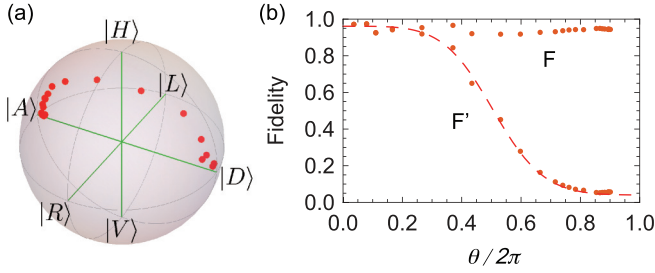
FIG. 3. (a) The Poincaré sphere (Bloch sphere) for the polarization state of light. $|R\rangle$ ($|L\rangle$) is the right (left) circular polarization state. The trajectory of the states from $\theta = 0$ to $\theta \sim 2\pi$ is represented by red circles from near $|D\rangle$ to $|A\rangle$. (b) $\theta(P)$ dependencies of fidelities F and F'. The dashed curve is theoretically obtained by using experimental parameters.

Fig. 2(e). The best fit to the data with a Gaussian gives the FWHM of 0.36 nm corresponding to 176 GHz. This value is in good agreement with the intrinsic bandwidth 0.3 nm (about 150 GHz) of the PPLN without the cavity [13]. We thus conclude that the cavity-enhanced broadband photonic Rabi oscillation was surely achieved.

B. Polarization rotation by photonic Rabi oscillation

The photonic Rabi oscillation can be used for the polarization rotation of the signal light. The experiment for such an operation was performed by the same setup in Fig. 1(c). The input signal light at 780 nm is set to diagonal polarization whose state is written as $|D\rangle := (|H\rangle + |V\rangle)/\sqrt{2}$, where $|H\rangle$ and $|V\rangle$ are states for the horizontal and V polarization of light, respectively. Because only the V-polarized light is frequency converted by the type-0 quasi-phase-matched PPLN/WR, the polarization state of the light at 780 nm is transformed into $|\psi_\theta\rangle := \mathcal{N}(|H\rangle + \cos\frac{\theta}{2}|V\rangle)$ ideally, where $\mathcal{N} := (1 + \cos^2\frac{\theta}{2})^{-1/2}$ is the normalization constant. For 780 nm light coming from the PPLN/WR, the polarization state tomography was performed by inserting a polarization analyzer composed of a quarter wave plate, a HWP, and a polarizing BS into the optical path just before PD_e.

In Fig. 3(a), we show the trajectory of the polarization states on the Poincaré sphere (or Bloch sphere) estimated from Stokes parameters. As the pump power increases, the initial state near $|\psi_0\rangle(= |D\rangle)$ is transformed towards $|\psi_{2\pi}\rangle = |A\rangle := (|H\rangle - |V\rangle)/\sqrt{2}$, via a state near $|\psi_\pi\rangle = |H\rangle$. For quantitative evaluation of the rotation, we borrowed the density operator representation ρ_θ of the polarization state for various values of $\theta = \theta(P)$ from the quantum information theory. We evaluated the fidelities $F := \langle\psi_\theta|\rho_\theta|\psi_\theta\rangle$ of ρ_θ to the ideal state $|\psi_\theta\rangle$ and $F' := \langle\psi_0|\rho_\theta|\psi_0\rangle$ of the states with turning on and off the pump light. The results are shown in Fig. 3(b). For every θ, F is higher than 0.9, and thus the polarization state is successfully rotated by the Rabi oscillation for any pump power with a resonant frequency. The result of F', which approaches zero as θ increases, also shows the rotation effect. We notice that for $\theta \sim 2\pi$ achieved by $P \sim 340\,\text{mW}$, F' is close to zero due to the effect of the geometric phase added through the full Rabi cycle [29–31]. The above polarization rotation was controlled by amplitude modulation (AM) of the

pump light at a frequency resonant to the cavity. In addition to the AM control, the cavity structure enables us to toggle the polarization rotation by frequency modulation (FM) of the pump light between off-resonant and on-resonant conditions with a fixed pump power.

We construct a theoretical model for the state transformation by the photonic Rabi oscillation. The observed maximum transition efficiency is $A = 0.95$. We assume that the imperfection is originated from the propagation mode mismatch of the signal and the pump light. We denote the propagation mode which interacts with the pump light by $|x\rangle$ and its orthogonal mode by $|\bar{x}\rangle$. Under the assumption, when the input state is a pure state with diagonal polarization, the initial state to the device can be written as $|\psi_{\text{in}}\rangle := |D\rangle(\sqrt{A}|x\rangle + \sqrt{1-A}|\bar{x}\rangle)$. After the Rabi oscillation with θ, the normalized output state $|\psi_{\text{out}}\rangle$ is ideally described by

$$|\psi_{\text{out}}\rangle := \mathcal{N}_0(\sqrt{A}\mathcal{N}^{-1}|\psi_\theta\rangle|x\rangle + \sqrt{2(1-A)}|D\rangle|\bar{x}\rangle), \quad (2)$$

where $\mathcal{N}_0 := (A\mathcal{N}^{-2} + 2(1-A))^{-1/2}$ is a normalization factor. In our experiment, the reconstructed states ρ_θ were slightly impure, namely $\text{Tr}(\rho_\theta^2) < 1$. We model the output state including the impurity as $\rho_{\text{th}} := p|\psi_{\text{out}}\rangle\langle\psi_{\text{out}}| + (1-p)I/2$, where $p := (2\langle\text{Tr}(\rho_\theta^2)\rangle - 1)^{1/2}$ and I is the identity operator. By using experimentally observed values $A = 0.95$ and $\langle\text{Tr}(\rho_\theta^2)\rangle = 0.93$, we obtained the fidelity $F_{\text{th}} := \langle\psi_{\text{in}}|\rho_{\text{th}}|\psi_{\text{in}}\rangle$ as shown in Fig. 3(b). We see that the experimental results are in good agreement with the curve theoretically predicted with the use of the experimental parameters.

V. DISCUSSION

In our demonstration for the polarization state rotation, we measured only the polarization state of 780 nm light. When we consider the frequency DOF composed of 780 nm and 1522 nm modes, which we denote by $|\omega_{\text{h}}\rangle$ and $|\omega_{\text{l}}\rangle$, the photonic Rabi oscillation system will work on a single-photon two-qubit state [32] formed by the polarization and the frequency modes of the single photon. Because the PPLN/WR has polarization dependency, an input state $|D\rangle|\omega_{\text{h}}\rangle$ is deterministically transformed into the single-photon Bell states as $(|H\rangle|\omega_{\text{h}}\rangle \pm |V\rangle|\omega_{\text{l}}\rangle)/\sqrt{2}$ by the Rabi oscillation with $\theta = \pi/4$ and $3\pi/4$. These operations correspond to the controlled NOT gates. Combining frequency-dependent WPs, the other two Bell states can be easily generated. The measurement of the four Bell states is also deterministically achieved by the same setup. These two-qubit gates can be used for the manipulation of hyperentangled states. For example, starting from a conventional n-photon GHZ state $(|H\rangle^{\otimes n} + |V\rangle^{\otimes n})|\omega_{\text{h}}^{\otimes n}\rangle/\sqrt{2}$, by applying the above gates to n photons, the hyperentangled GHZ state [33] written as $(|H\rangle^{\otimes n}|\omega_{\text{h}}\rangle^{\otimes n} + |V\rangle^{\otimes n}|\omega_{\text{l}}\rangle^{\otimes n})/\sqrt{2}$ can be generated.

VI. CONCLUSION

In conclusion, we have demonstrated cavity enhancement of photonic Rabi oscillation while keeping the flexible choice of frequencies and wide acceptance bandwidths of photons. The enhancement of the nonlinear optical coupling was 10 times larger than conventional frequency converters. This leads to the observation of the full Rabi cycle between the two photonic frequencies, resulting in all-optical versatile

manipulation beyond the frequency DOF. Our results will open up a large-scale photonic quantum information processing based on frequency modes including hyperentangled systems [34,35]. Furthermore, considering several two-level virtual systems as shown in Fig. 1(a) and their interaction by using multiple pump lasers with proper frequency detunings, there is a possibility that such a photonic system would simulate and design complicated atomic systems including more than two virtual energy levels. Our experiments have been performed with pump frequency scanning as in conventional nonlinear systems with cavity enhancement. For a stable operation of the device, the use of a laser frequency locking system such as reported in Ref. [27] is important because the pump frequency fluctuations would degrade the average transition efficiency and the purity of the output state.

[1] W. McGrew *et al.*, Nature (London) **564**, 87 (2018).

[2] K. Bongs *et al.*, Nat. Rev. Phys. **1**, 731 (2019).

[3] H. J. Kimble, Nature (London) **453**, 1023 (2008).

[4] J. I. Cirac and P. Zoller, Nature (London) **404**, 579 (2000).

[5] I. S. Madjarov *et al.*, Nat. Phys. **16**, 857 (2020).

[6] P. Kumar, Opt. Lett. **15**, 1476 (1990).

[7] T. Kobayashi *et al.*, Nat. Photonics **10**, 441 (2016).

[8] S. Clemmen, A. Farsi, S. Ramelow, and A. L. Gaeta, Phys. Rev. Lett. **117**, 223601 (2016).

[9] C. Joshi, A. Farsi, A. Dutt, B. Y. Kim, X. Ji, Y. Zhao, A. M. Bishop, M. Lipson, and A. L. Gaeta, Phys. Rev. Lett. **124**, 143601 (2020).

[10] M. Y. Niu, I. L. Chuang, and J. H. Shapiro, Phys. Rev. Lett. **120**, 160502 (2018).

[11] M. Y. Niu, I. L. Chuang, and J. H. Shapiro, Phys. Rev. A **97**, 032323 (2018).

[12] S. Krastanov *et al.*, Nat. Commun. **12**, 191 (2021).

[13] R. Ikuta *et al.*, Nat. Commun. **2**, 537 (2011).

[14] B. Albrecht, P. Farrera, X. Fernandez-Gonzalvo, M. Cristiani, and H. De Riedmatten, Nat. Commun. **5**, 3376 (2014).

[15] R. Ikuta *et al.*, Nat. Commun. **9**, 1997 (2018).

[16] M. Bock *et al.*, Nat. Commun. **9**, 1998 (2018).

[17] A. Dréau, A. Tchebotareva, A. E. Mahdaoui, C. Bonato, and R. Hanson, Phys. Rev. Appl. **9**, 064031 (2018).

[18] Y. Yu *et al.*, Nature (London) **578**, 240 (2020).

[19] T. vanLeent, M. Bock, R. Garthoff, K. Redeker, W. Zhang, T. Bauer, W. Rosenfeld, C. Becher, and H. Weinfurter, Phys. Rev. Lett. **124**, 010510 (2020).

[20] X. Guo, C.-L. Zou, H. Jung, and H. X. Tang, Phys. Rev. Lett. **117**, 123902 (2016).

[21] X. Lu *et al.*, Nat. Photonics **13**, 593 (2019).

[22] M. Kues *et al.*, Nat. Photonics **13**, 170 (2019).

[23] R. Ikuta, R. Tani, M. Ishizaki, S. Miki, M. Yabuno, H. Terai, N. Imoto, and T. Yamamoto, Phys. Rev. Lett. **123**, 193603 (2019).

[24] D. F. Walls and G. J. Milburn, *Quantum Optics* (Springer Science & Business Media, Berlin, Heidelberg, 2007).

[25] R. Ikuta *et al.*, Opt. Express **21**, 27865 (2013).

[26] R. Regener and W. Sohler, JOSA B **5**, 267 (1988).

[27] M. Stefszky *et al.*, J. Opt. **20**, 065501 (2018).

[28] R. Ikuta, M. Asano, R. Tani, T. Yamamoto, and N. Imoto, Opt. Express **26**, 15551 (2018).

[29] A. P. VanDevender and P. G. Kwiat, Opt. Express **15**, 4677 (2007).

[30] N. K. Langford *et al.*, Nature (London) **478**, 360 (2011).

[31] A. Karnieli, S. Trajtenberg-Mills, G. Di Domenico, and A. Arie, Optica **6**, 1401 (2019).

[32] Y.-H. Kim, Phys. Rev. A **67**, 040301(R) (2003).

[33] W.-B. Gao *et al.*, Nat. Phys. **6**, 331 (2010).

[34] J. T. Barreiro, T.-C. Wei, and P. G. Kwiat, Nat. Phys. **4**, 282 (2008).

[35] C. Reimer *et al.*, Nat. Phys. **15**, 148 (2019).